glacies

Article

Evolution and Controls of the Large-Scale Surface Freeze-Back Onset in Siberian Permafrost Regions with the ERA5-Land Reanalysis

Cécile Osy [1], Sophie Opfergelt [2], Arsène Druel [3] and François Massonnet [1,*]

[1] Earth and Climate Research Center, Earth and Life Institute, Université catholique de Louvain, 1348 Louvain-la-Neuve, Belgium; cecile.osy@uclouvain.be
[2] Environmental Sciences, Earth and Life Institute, Université catholique de Louvain, 1348 Louvain-la-Neuve, Belgium; sophie.opfergelt@uclouvain.be
[3] Ecologie des Forêts Méditerranéennes (URFM), INRAe, 84000 Avignon, France; arsene.druel@gmail.com
* Correspondence: francois.massonnet@uclouvain.be

Abstract

Permafrost is a defining feature of the Arctic and sub-Arctic environments. The extent of the permafrost region accounts for about a quarter of the Northern Hemisphere's terrestrial surface. While most research on permafrost has focused on the summer season—when the active layer is thawed and carbon emissions peak—the late shoulder season, marking the transition season between summer and winter and ending by surface freeze-back at the large scale, has received less attention. Yet, about 14% of the annual mean methane emissions from the permafrost occur during the refreezing period of the active layer. Understanding the seasonality, interannual variability and long-term trends of the surface freeze-back is therefore crucial to better constrain the high-latitude atmospheric carbon budget and improve Earth System Model projections. In this study, we analyze the evolution of surface freeze-back onset from 1950 to 2020 using the ERA5-Land reanalysis (0.1° spatial resolution) over a large region of Siberia encompassing the four main permafrost types. We find that surface freeze-back onset has been delayed by five days on average over that 70-year period. Through spatial regression modeling, we show that while several climatic and geographic factors influence freeze-back timing, the principal control on freeze-back seasonality at the large scale (~kilometers) is the date when the 2 m air temperature first falls below 0 °C, followed by the snow cover depth. These findings complement previous research that focused on the small scale (~meters), which emphasized the importance of the vegetation type and the snow cover characteristics at these spatial scales. Our results provide new insights into changes during the late shoulder season in one of the world's fastest-warming regions and identify key variables to monitor for improving sub-seasonal forecasts that could become relevant to infrastructure upgrade and logistics planning in permafrost-affected areas.

Keywords: permafrost; polar climate; freeze-back onset

Academic Editor: Adriano Ribolini

Received: 31 July 2026
Revised: 8 September 2026
Accepted: 17 September 2026
Published: 22 September 2026

1. Introduction

The region of permafrost—ground that remains at or below 0 °C for at least two consecutive years—covers about one quarter of the land surface in the Northern Hemisphere [1,2]. Permafrost stores approximately twice as much carbon as is currently present in the atmosphere, i.e., an estimated 1400–1600 GtC [3]. In the Arctic region, where air temperatures have been rising two to four times the global average—a phenomenon known as Arctic amplification [4–6]—significant increases in permafrost temperatures have been recorded in the upper 30 m over the past three to four decades [7]. Moreover, under current emission scenarios, the extent of near-surface (3–4 m) permafrost is expected to decline by 24–69% relative to the 1986–2005 average value [8] and could even decline by 90% for high-end emission scenarios [9]. It is also estimated that the annual mean frozen volume in the top 2 m of soil could shrink by 10–40% per degree of global warming [10].

As permafrost warms and eventually thaws, it exposes previously frozen organic carbon to microbial decomposition, which in turn releases carbon in the form of carbon dioxide (CO_2) or methane (CH_4) depending on whether local conditions are aerobic or anaerobic [11]. The emission of these two potent greenhouse gases induces a positive radiative forcing on the Earth's energy balance that eventually leads to more surface warming and further permafrost thaw—a self-reinforcing process known as the permafrost-carbon feedback [12,13]. While the positive permafrost-carbon feedback has been identified as the key element in a potential tipping point involving the permafrost, there is currently no evidence of an acceleration of permafrost thaw on a large scale and the relationship between permafrost area and global mean temperature remains close to linear [14].

At the seasonal scale, permafrost carbon emissions peak during the summer when soil temperatures are highest, although microbial decomposition—and the resulting release of CO_2 and CH_4—can continue even under cold conditions [15,16]. The late shoulder season (the period starting after plant senescence and ending by surface freeze-back; Figure 1) deserves particular attention for two reasons. First, its end determines the refreezing of the active layer which accounts for a non-negligible 14% of the annual mean CH_4 emissions [17]. Second, it coincides with the seasonal peak of Arctic amplification, as air and ground temperatures have been observed to rise most rapidly from late summer to early winter [6,18]. As a result, accurately identifying the onset of surface freeze-back—and how it evolves in a warming climate—is key to understanding the seasonality of permafrost carbon emissions in present and future conditions.

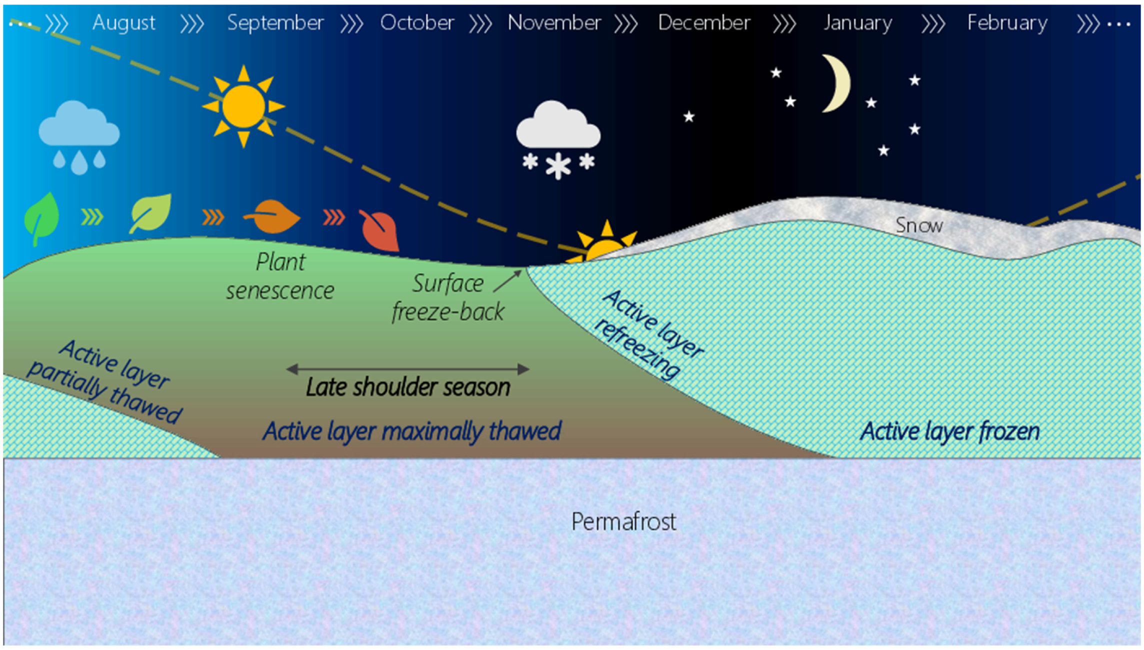

Figure 1. Conceptual scheme of the seasonal transition between summer and winter with the late shoulder season marking the transition between plant senescence and surface freeze-back, and the active layer refreezing period. Note that the figure is not to scale and misses many characteristics such as the seasonality of methane fluxes.

With the many observed shifts in Arctic climate indicators, it is reasonable to hypothesize that the onset of the surface freeze-back has also undergone significant changes. However, fine-scale observations in permafrost-covered regions—e.g., typically collected at meter-scale resolution [19]—lack the spatial coverage needed to determine whether local changes also occur at broader spatial scales, on the order of kilometers. Moreover, long-term and temporally consistent datasets suitable for climate-scale analyses remain scarce or altogether absent. Consequently, the evolution of the onset of surface freeze-back remains poorly documented and has yet to be comprehensively characterized or quantified. In addition, permafrost studies exhibit a strong seasonal bias, with far more observations collected between June and August than during the transitional (spring and autumn) and cold (winter) seasons, primarily due to accessibility constraints [17,20]. While year-round ground temperature time series exist at, e.g., several monitoring sites [21–23], their localized nature limits their representativeness for broader regions. Consequently, no robust conclusions can yet be drawn about long-term trends in the timing of freeze-back at interannual or interdecadal time scales across large spatial domains.

Several knowledge gaps and research questions thus remain open: What is the year-to-year variability in the onset of surface freeze-back? Are long-term trends detectable? Can these trends be linked to specific climatic and geographic contexts? These questions form the backbone of this study. The specific objectives of this work are (i) to investigate the evolution of the onset of surface freeze-back over the past 70 years and (ii) to identify the main controls of observed changes and quantify their relative contributions. In the following section (Section 2: Methodology), we review the datasets, variables, study area and statistical models used to address these questions. We then present the trends in the onset of surface freeze-back and their relationship with key variables (Section 3: Results). We discuss the limitations of the study in Section 4 (Discussion) before concluding (Section 5: Conclusions).

2. Materials and Methods

2.1. Study Area

The study area (45–65° N; 95–125° E) is located in Siberia, Russia (Figure 2). It covers approximately 4.2 million km^2 and encompasses all four main permafrost zones, classified by the proportion of the ground underlain by permafrost: continuous (>90%), discontinuous (50–90%), sporadic (10–50%), and isolated (<10%), following the dataset of ref. [24] which maps permafrost extent across the Northern Hemisphere at 1 km resolution for the period 2000–2016. The broad spatial coverage ensures sufficient sampling across all zones to support statistically robust conclusions.

2.2. ERA5-Land

This study employs the ERA5-Land dataset [25] as the primary source of information to address the research questions outlined in the introduction. ERA5-Land is the land component of the fifth-generation European ReAnalysis (ERA5; ref. [26]) produced by the European Center for Medium-Range Weather Forecasts (ECMWF). It provides high-frequency (1 h), global, high-resolution (~9 km) data generated by numerical integrations of ECMWF's land surface model (the Carbon-Hydrology-Tiled ECMWF Scheme for Surface Exchanges over Land; CHTESSEL). The land surface model is driven by downscaled atmospheric forcing derived from the ERA5 reanalysis. While ERA5-Land does not assimilate land observations directly, the land surface evolution is indirectly influenced by observations through the atmospheric forcing. The near-surface thermodynamic fields are also corrected for ground elevation. The dataset is available from 1950 to present.

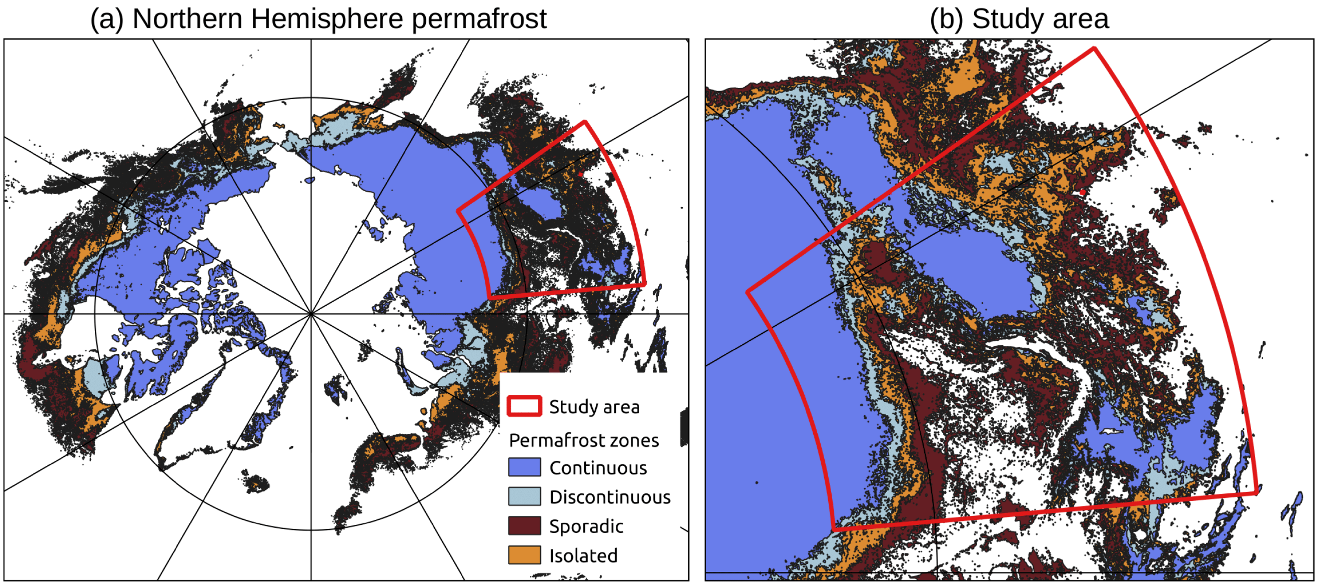

Figure 2. Maps of (**a**) the Northern Hemisphere and (**b**) the study area highlighting the four different permafrost zones defined following the classification of ref. [24]).

The CHTESSEL model used in ERA5-Land solves energy and mass conservation equations to prognostically calculate key land state variables, including soil temperature and snow cover. Compared to earlier model versions, ERA5-Land accounts for more comprehensive snow-related processes, such as changes in density due to overburden and thermal metamorphism, which eventually affects the snow cover fraction [27]. Soil heat fluxes are modeled by Fourier's law and the soil column is discretized into four layers: 0–7 cm, 7–28 cm, 28–100 cm, and 100–289 cm. Vegetation and land surface characteristics are prescribed as time-invariant fields, meaning that soil type, vegetation type and vegetation cover are based on annually repeating climatologies [25].

The choice of ERA5-Land dataset for this study reflects a trade-off between long-term availability, high temporal resolution, global coverage, and physical consistency. Although field observations could have offered greater realism at specific locations, they lack the spatial coverage needed for robust analyses across all permafrost zones and geographical regions. Satellite remote sensing data provides broader spatial coverage but does not include all variables relevant to this study. ERA5-Land offers a good balance between these two options by proposing a consistent and comprehensive dataset. It has shown reasonable agreement with independent in situ observations and has demonstrated improved performance over its predecessors, especially at high latitudes [25]. However, it is not without limitations—for example, issues have been reported in hydrological modeling in the Alpine region [28] and systematic temperature biases have been identified in permafrost areas [27]. We return to the limitations of ERA5-Land in the context of our research questions in Section 4 (Discussion).

2.3. Diagnosing the Onset of Surface Freeze-Back

Our diagnosis of the onset of surface freeze-back is based on the date when the daily mean ground temperature in the first layer (0–7 cm) of ERA5-Land drops below the 0 °C threshold. Daily mean ground temperature is defined as the arithmetic average of the temperature at 00:00 and 12:00 UTC. Due to short-term meteorological fluctuations, the 0 °C threshold may be crossed several times before onset of sustained winter freezing. To filter out this high-frequency variability and avoid detecting temporary freezing events, we apply a 15-day moving average (centered and with equal weighting across days) to the daily time series. From the smoothed time series, we identify, for each grid cell and each year, the first date (counted as days elapsed since 1 July) when the temperature drops below 0 °C, marking the onset of persistent surface freeze-back.

The dates of surface freeze-back serve as the predictands (i.e., as our prediction targets) in our spatial prediction model developed in Section 2.4. For the trend analysis (Section 3.1), these dates are aggregated at the scale of the entire study area or by permafrost type, using area-weighted averages across all grid cells. The trend and uncertainty around it are estimated through an ordinary least square regression without considering temporal autocorrelation.

2.4. Spatial Regression Model for the Onset of Surface Freeze-Back

To interpret the year-to-year, long-term, and spatial variability of the onset of surface freeze-back, we use a spatial regression model. A spatial regression model is a variant of a multilinear regression model that includes an additional error structure to account for spatial autocorrelation—both among the independent variables and within the residuals. The spatial model used in this study has been implemented using the spreg package in Python 3.10.8 (https://pysal.org/spreg/; accessed on 10 October 2024). Specifically, a Generalized Method of Moments (GMM) estimator has been used that handles both homoscedastic and heteroskedastic errors. The spatial model is defined by the following two equations [29]:

$$\boldsymbol{y} = \boldsymbol{X}\boldsymbol{\beta} + \boldsymbol{e} \tag{1}$$

with

$$\boldsymbol{e} = \boldsymbol{\omega}\boldsymbol{W}\boldsymbol{u} + \boldsymbol{\epsilon} \tag{2}$$

In Equation (1), $\boldsymbol{y} = (y_1, y_2, \ldots y_n)$ is an $n \times 1$ vector containing the onset dates of surface freeze-back (as defined in Section 2.3), where n is the number of grid cells in the study area. $\boldsymbol{X}$ is a $n \times m$ matrix of m independent variables (predictors, see Section 2.5) of length n, each arranged in a column. $\boldsymbol{\beta}$ is an $m \times 1$ vector of parameters (or regression coefficients), and $\mathbf{e}$ is the $n \times 1$ vector representing the error term.

Equation (2) decomposes $\boldsymbol{e}$ into two components: an $n \times 1$ random vector of random errors $\boldsymbol{\epsilon} = (\epsilon_1, \epsilon_2, \ldots \epsilon_n)$, and a spatially structured component $\boldsymbol{\omega}\boldsymbol{W}\boldsymbol{u}$. Here, $\boldsymbol{\omega}$ $(n \times m)$ is a spatial error coefficient; $\boldsymbol{u}$ $(m \times 1)$ is the original unstructured error term, and $\boldsymbol{W}$ is the spatial weight matrix $\boldsymbol{W}$ (sparse $m \times m$ matrix) encoding the spatial structure. These spatial weights were defined using a Queen contiguity criterion, whereby grid cells sharing either an edge or a corner were considered neighbors. Grid cells containing missing values were excluded. The matrix was standardized so that the weights assigned to the neighbors of each grid cell summed to one. The suitability of a spatial error model over a standard linear model was confirmed using a Lagrange multiplier test [29,30], which indicated significant spatial dependence on the residuals (the Lagrange multiplier test is not shown here).

2.5. Candidate Predictors

The onset of surface freeze-back depends on several factors, hereafter referred to as "predictors", some of which are used in the spatial regression model described in the previous section. We describe below the candidate predictors considered in this study, along with their data sources and post-processing steps.

2.5.1. Vegetation Type

The type of vegetation is a first potential predictor of the onset of surface freeze-back. Environmental stress associated with Arctic climate change has led to modifications of the Arctic flora [31–33]. These modifications include widespread increases in vegetation biomass over recent decades in multiple areas across the Arctic [31,34]. Vegetation plays a key role in surface soil properties, through temperature and moisture variations. In addition, the shading caused by vegetation mitigates evaporation and therefore mitigates the risk of extreme heat events [35–38]. The plant canopy also modifies the local albedo and changes snow interception in winter, and thus influences the surface characteristics including its energy balances [39–42].

Vegetation type data were obtained from the Global Land Cover 2000 database (https://forobs.jrc.ec.europa.eu/glc2000, accessed on 10 October 2024) and aggregated to a 1° resolution based on the mode—the most frequently occurring vegetation type within the grid cell. The choice of 1° resolution is aimed at calculating the dominant type of vegetation for detecting the influence of this variable on the date of the onset of surface freeze-back. Aggregating the high-resolution (~1 km) data to 0.1° would have produced highly variable space data. Land cover types were then reclassified in three categories: "less insulating" (taller vegetation not covering the ground), "more insulating" (low-lying vegetation) and "unclassified" (Table 1). This classification is based on the literature suggesting that ground-level vegetation provides greater thermal insulation than taller and sparse vegetation [35,38,41,43–46]. The reclassification vegetation type is included in the spatial model as a static categorical (logistic) variable.

Table 1. Mapping between the vegetation type available from the Global Land Cover 2000 database and the assigned logistic regression variable in the spatial regression model ("less insulating", "more insulating", "unclassified").

Less Insulating	More Insulating	Unclassified
Forest	Humid grasslands	Recent burns
Evergreen needleleaf	Steppe	Burns of year 2000
Deciduous broadleaf	Palsa bog	Unclassified
Needleleaf/broadleaf	Riparian vegetation	
Mixed	Prostrate shrub tundra	
Broadleaf/Needleleaf	Sedge tundra	
Deciduous needleleaf	Bogs and marshes	
Broadleaf deciduous shrubs	Cropland–grassland complexes	
Forest–natural vegetation complexes	Croplands	
Evergreen needleleaf shrubs	Permanent snow/ice	
Urban	Water bodies	
Barren tundra	Salt marsh	
Shrub tundra		
Forest–cropland complexes		
Bare soil and rock		

Despite some caveats, this classification offers sufficient insight to address our scientific questions. Vegetation data is only available for a single year (2000) but were used as a proxy for the entire study period (1950–2020). While we acknowledge an ongoing Arctic greening trend [47,48], this assumption was made to focus on the spatial rather than the temporal variability of this predictor.

2.5.2. Volumetric Soil Water Content

Volumetric soil water content is a second variable that may influence the onset of the surface freeze-back by affecting heat fluxes, as it represents a source of latent energy that must be released before freezing can occur. However, volumetric soil water content is controlled by multiple factors such as precipitation (and the nature of its phase), evaporation, drainage potential and active layer thickness. Permafrost inhibits drainage, often causing perched water tables [49], increased surface water runoff and reduced subsurface flow [50]. Changes in permafrost extent or active layer thickness—or both—can significantly alter ground hydrology [51]. Volumetric soil water content (volumetric soil water level 1 (0–7 cm); variable swvl1) was derived from the ERA5-Land dataset.

2.5.3. Snow Cover

Snow cover is a third key predictor of the onset of the surface freeze-back. Field studies have identified snow as a critical factor influencing permafrost dynamics [52–54]. Due to its low thermal conductivity, snow acts as an effective insulator [55]. The timing of snowfall is particularly important: if snow accumulates early in the season before ground temperatures drop below 0 °C, it can trap heat and delay freezing; by contrast, if snowfall occurs after ground freezing, it slows further heat loss and helps maintain cold soil conditions.

To capture the insulating effect of snow on the onset of surface freeze-back, we use the snow depth variable from ERA5-Land (variable sde) which provides twice-daily (00:00 and 12:00 UTC) snow thickness estimates from 1950 to 2020. Based on physical considerations, we seek to establish a critical snow depth h that would correspond to an effective insulation thickness. For this, we start from Fourier's law of heat conduction:

$$Q_{snow} = \frac{k\Delta T}{h} \tag{3}$$

where Q_{snow} is the conductive heat flux (W.m^{-2}) through snow; k is the snow thermal conductivity (W.m^{-1}.K^{-1}); ΔT is the temperature difference across the snow layer, and h is the snow depth. In the absence of snow, heat transfer between the ground and the atmosphere can be approximated by the sensible heat flux:

$$Q_{no\ snow} = \rho . c_{p,a} . \kappa . u . \Delta T \tag{4}$$

where ρ is the air density (taken as 1.225 kg.m^{-3}); $c_{p,a}$ is the air-specific heat (taken as 1000 J.kg^{-1}.K^{-1}); κ is the coefficient of transfer (dimensionless, taken as 0.01); u is the characteristic speed of friction (taken as 3 m.s^{-1}), and ΔT is the difference in temperature between the air and the ground. If we define an "insulating" snow layer as one that reduces the heat transfer to less than 5% of the value in the absence of snow, $Q_{snow}/Q_{no\ snow} < 0.05$, this would imply

$$h > \frac{k}{0.05\ \rho c_{pa} . \kappa . u} \tag{5}$$

For a typical snow cover with density of 350 kg.m^{-3}, conductivity k is equal to 0.25 W.m^{-1}.K^{-1} [56]. We therefore find that $h > 14$ cm corresponds to an insulating layer. Sensitivity Monte-Carlo sampling tests revealed that this value of 14 cm is relatively representative of average conditions when conductivity and wind speed are varied around their chosen values (Figure A1 from Appendix A). This threshold of snow thickness of 14 cm is finally used to define the day marking the presence of snow in a grid cell, day_{snow} (see Section 3.2). Values below that threshold correspond to the beginning of the winter with highly variable snow cover due to snowmelt events occurring during early winter (e.g., [57]).

2.5.4. Near-Surface Air Temperature

Near-surface air temperature (hereafter referred to as "surface temperature") also plays a direct role in the ground temperature fluctuations in the Arctic [23] and is therefore a control of the onset of surface freeze-back. Surface temperatures are influenced by different factors (e.g., cloud cover, heat advection by dominant winds, wind-driven turbulent heat fluxes at the surface) and their changes also influence other predictors (e.g., the phase of precipitation).

https://doi.org/10.3390/glacies3040013

Surface temperature data were extracted from the ERA5-Land dataset (2 m air temperature, variable 2t). As in Section 2.3, a 15-day moving average was applied to smooth out the high-frequency variability. The 0 °C threshold was then used to define the day marking the persistent cold air conditions (see Section 3.2).

2.5.5. Latitude

Latitude is finally an important time-invariant variable to consider for investigating the onset of the surface freeze-back since it controls the average insolation (amount of solar energy received at the Earth's surface per unit area and per unit of time) and its seasonal distribution, which in turn influence the type of permafrost.

We note that all the variables listed above are correlated to each other (e.g., latitude correlates with near-surface temperature and snow cover). While it is not possible to entirely remove the influence of this autocorrelation, the spatial regression model accounts for errors in the modeled variables.

3. Results

3.1. Temporal Evolution of the Onset of Surface Freeze-Back

The onset of surface freeze-back (as defined in Section 2.3) is averaged over the entire study area for each year. The resulting time series (Figure 3) shows a significant positive trend of +4.5 days over the 1950–2000 period (p-value < 0.01). Despite this statistically significant trend, year-to-year variability remains substantial: for example, the average surface freeze-back date differed by nearly two weeks between 1967 and 1968. Additionally, the spatial averages shown in Figure 3 mask considerable spatial variability at the grid-cell level. The ground in the grid cells situated in sporadic, isolated areas as well as the grid cells at the southern and western boundaries of the domain tend to freeze-back later than the average, while the areas of continuous permafrost tend to freeze-back earlier than the average (Figure A2 from Appendix A).

To further investigate regional differences and the role of spatial variability in the results, the study area was divided into four subareas corresponding to the four main permafrost zones. This allowed us to assess whether the trend reported in Figure 3 holds within each zone individually. When calculated by permafrost zone, the positive trend in the onset of the surface freeze-back remains positive (Figure 4). Notably, the trend is weakest in areas of continuous permafrost (+3.3 [0.4–6.3] days). Among other factors, the ground in these permafrost regions might be less responsive to atmospheric forcing than in other permafrost regions due to lower ground temperatures (for a constant ground ice content). However the role of the snow cover as thermal insulator should also be taken into account [58]. In contrast, the trends in isolated (+5.1 [1.8–8.5] days), sporadic (+5.4 [2.5–8.4] days) and discontinuous (+5.2 [2.4–8.0] days) permafrost are stronger and more similar to each other in magnitude because the ground is likely more responsive to the atmospheric forcing. Finally, high co-variability is also noticed among the four time series of the date of surface freeze-back across the four permafrost regimes (Figure 4). This suggests that the large-scale atmospheric controls are the primary cause for the year-to-year variability in the surface freeze-back.

3.2. Controls of the Onset of Surface Freeze-Back

The spatial regression model (Section 2.4), used to identify the key factors influencing the onset of the surface freeze-back, is applied on the candidate variables listed in Section 2.5. In contrast to the analysis of year-to-year variability of the previous section where the onset of surface freeze-back was averaged over space, the variables used to identify the controls of freeze-back onset were averaged over time (1950–2020). This approach was chosen to isolate the role of spatial variability by excluding the influence of temporal fluctuations that could have acted as a confounding factor in the analyses.

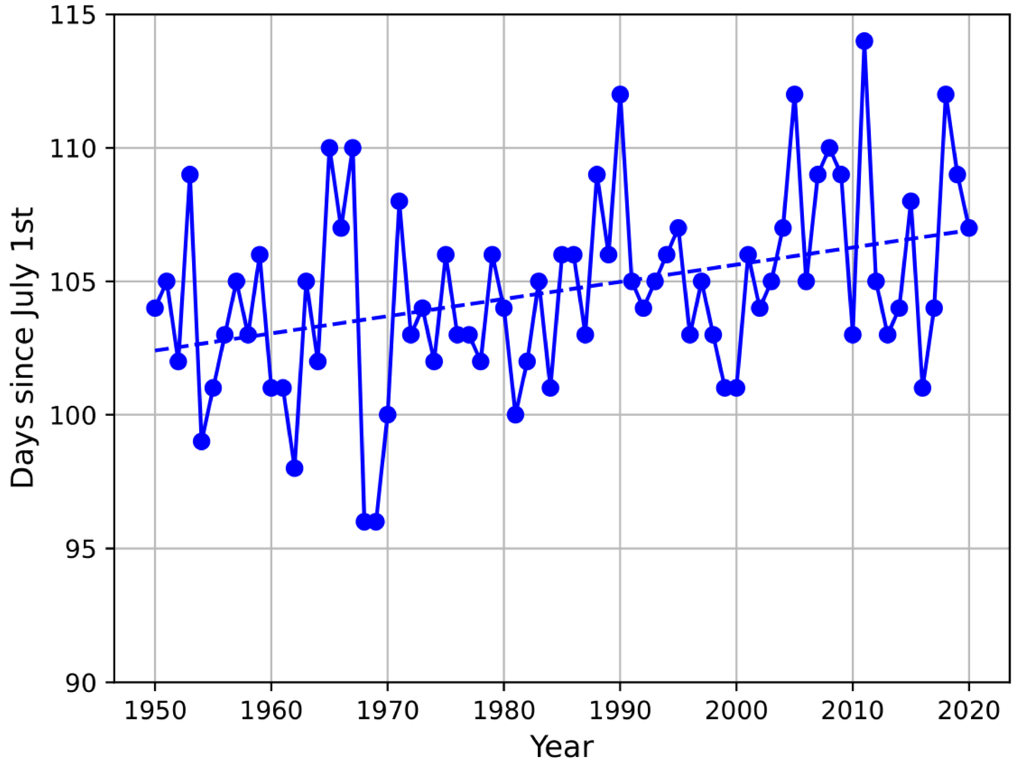

Figure 3. Evolution of the average date (counted as days since 1 July) of surface freeze-back in the study area (solid lines) and the corresponding linear trend (dashed line), according to the ERA5-Land dataset.

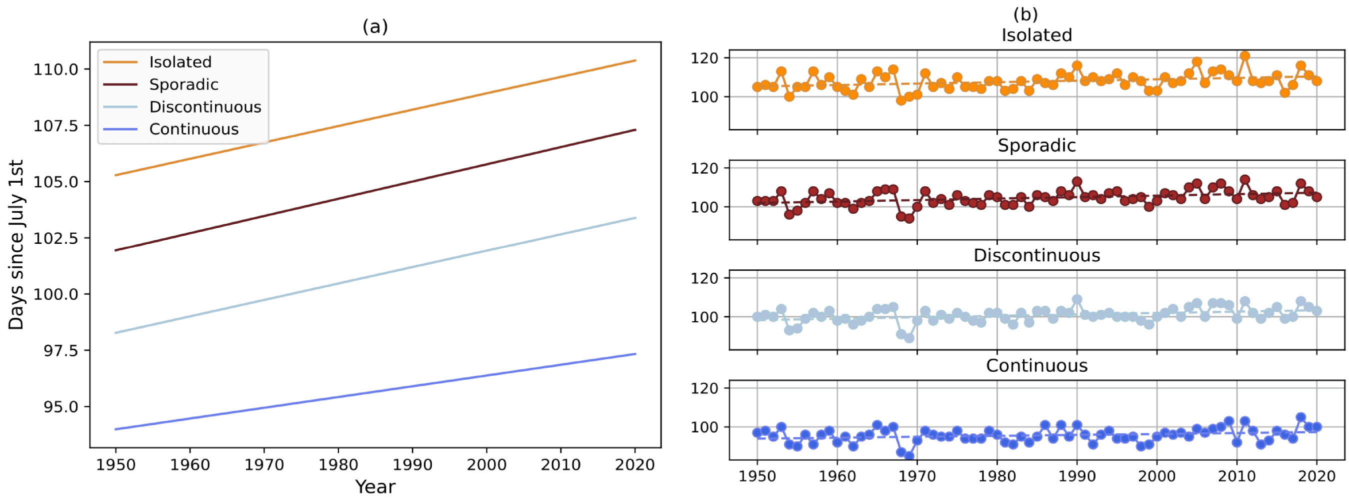

Figure 4. (**a**) Comparison between the trends in the onset of freeze-back (same conventions as in Figure 3) for the trend in the day between 1950 and 2020 (p-value = 0.01 for isolated, sporadic and discontinuous permafrost; p-value = 0.03 for continuous permafrost). (**b**) Detailed evolution between 1950 and 2020 of the day of the onset of the surface freeze-back for the different permafrost zones. The y-axes limits are identical for easier comparison.

To train the spatial error model, approximately 90% of the ERA5-Land data (55,501 out of 60,501 grid cells) were randomly selected and evenly distributed across the study area. This sampling strategy preserves a portion of the data for out-of-sample model validation. The remaining dataset was used for verification, allowing for an independent assessment of model skill. The random 90/10 split is used since the spatial heterogeneity of the permafrost zones within the study area prevents use of blocked cross-validation. Grouping similar structural units together through blocking may inadvertently remove unique features and introduce extrapolation issues [59]. Model performance was evaluated over the entire study area as well as separately for each of the four permafrost zones.

The model applied to the entire study area yields

$$day_{onset} = 0.05 - 0.08 \times day_{snow} + 1.02 \times day_{air\ temp.} \quad (6)$$

where the "*day*" variables are the number of days since 1 July for the onset of surface freeze-back, the snow depth exceeding 14 cm, and the air temperature dropping below 0 °C, respectively. The vegetation type, volumetric soil water content (in July) and latitude were found to be non-significant covariates (p-value > 0.05) and so were not included in Equation (6). The coefficients shown in Equation (6) are those obtained by running the model for a second time without those non-significant covariates. The negative sign associated with day_{snow} indicates that when it takes longer for the snow cover to exceed the given threshold of 14 cm, the onset of freeze-back occurs sooner; likewise, the rapid formation of an insulating snow cover delays the freeze-back. This relationship reflects the expected physical role of the insulator played by the snow.

To assess the predictive power of the model and to ensure it is not overfitting, we apply it to the ~10% of the data that were withheld during training. That is, we provide as inputs day_{snow} and $day_{air\ temp.}$ to Equation (6) and compare the predicted values for day_{onset} to the actual values derived from ERA5-Land. The resulting scatterplot (Figure 5) shows strong agreement between predicted and observed values, and the coefficient of determination (R^2 = 0.78) confirms the model's good predictive skill.

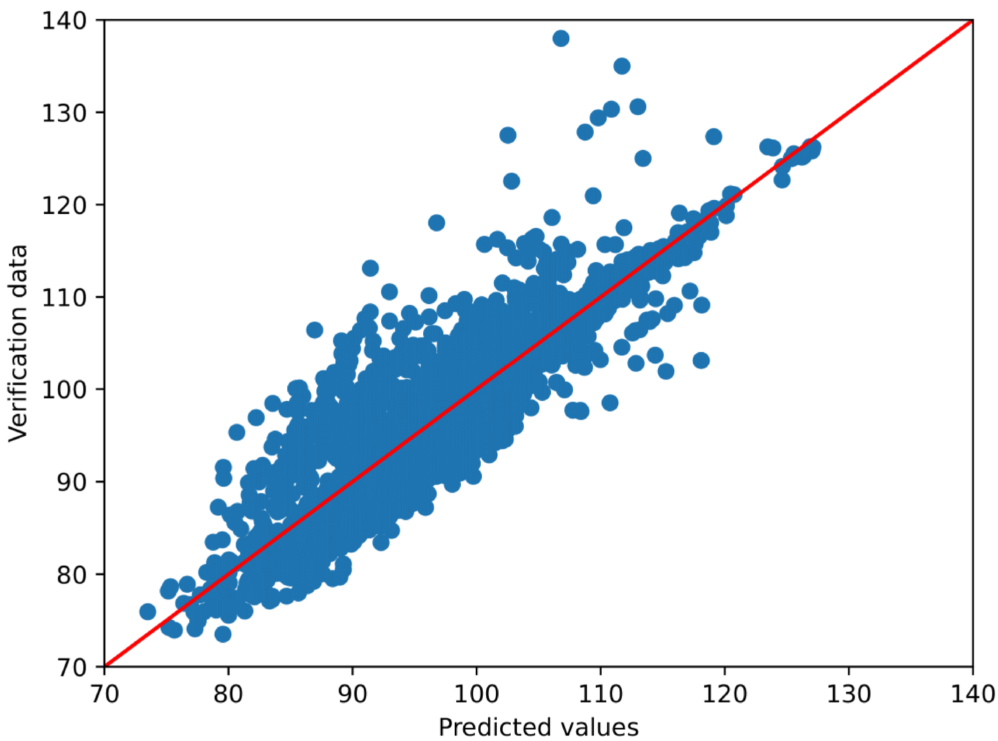

Figure 5. Predicted (x-axis, using Equation (6)) versus observed (y-axis) onset of surface freeze-back in the ERA5-Land dataset (counted from 1 July).

To further investigate spatial differences, the analysis was then repeated by permafrost zone. Permafrost type is a spatially autocorrelated variable (Figure 2) and represents a relevant statistical predictor in its own right, as it influences key ground properties. The standardized regression equations derived for each permafrost zone are presented in Table 2. Even if providing uncertainties on the coefficients would be valuable in the future to better assess the limit of the model, we propose a first evaluation of the importance of the variables based on these coefficients.

Unlike the model for the entire area, vegetation was found this time to be a significant predictor (except over continuous permafrost) of the day of surface freeze-back.

The standardized regression equations' coefficients in Table 2 reveal that both the timing of the 14 cm snow layer and the drop in 2 m air temperature below 0 °C are key predictors of surface freeze-back onset across all permafrost zones. Among these, the timing of the temperature drop consistently exhibits the largest and most significant coefficient, followed by the timing of the insulating snow cover. Vegetation is also a significant predictor in all zones except continuous permafrost where it is not significant. Both the snow and vegetation coefficients are negative, indicating that an early formation of an insulating snow cover delays the onset of surface freeze-back (as we expect), and that the ground beneath insulating vegetation (e.g., grasslands) tends to freeze later in the season.

Table 2. Coefficients for the spatial regression model (Equation (1), β) for the different variables (X) for each permafrost zone. Latitude and volumetric soil water content were found to be systematically non-significant and hence excluded from the analysis. To ensure an easy comparison, the variables in Equation (1) have been first standardized ((value-mean)/standard deviation).

	Constant Offset	Air Temperature	Snow Cover	Vegetation
Isolated	0.06	0.98	−0.22	−0.07
Sporadic	0.08	1.08	−0.42	−0.06
Discontinuous	0.03	1.06	−0.53	−0.12
Continuous	0.12	0.93	−0.29	Not significant

We finally repeat the scatterplot analysis for the four main zones. When analyzing the four permafrost zones separately, scatterplots comparing predicted values (from the equations in Table 2) to observed values from the verification dataset (the 10% withheld from training) show correlations ranging from 0.51 to 0.80, depending on the zone. Specifically, the correlation coefficients are 0.76 for continuous, 0.51 for discontinuous, 0.74 for sporadic, and 0.80 for isolated permafrost (Figure 6). The lower correlation coefficient for the discontinuous permafrost zone (0.51) relative to the other permafrost zones likely reflects a higher surface heterogeneity (microtopography and hydrological conditions) in the discontinuous permafrost zone than in other permafrost zones. For the microtopography, continuous permafrost presents limited features of subsidence such as water tracks, whereas as their presence increases and is more variable in discontinuous permafrost [60–62]. For the hydrological conditions, continuous permafrost leads to limited hydrological connectivity restricted to the surface, whereas discontinuous permafrost can present more variable hydrological conditions, such as diffuse hydrology in peatlands, or pulses of hydrological connectivity when the bedrock prevents vertical infiltration [63].

https://doi.org/10.3390/glacies3040013

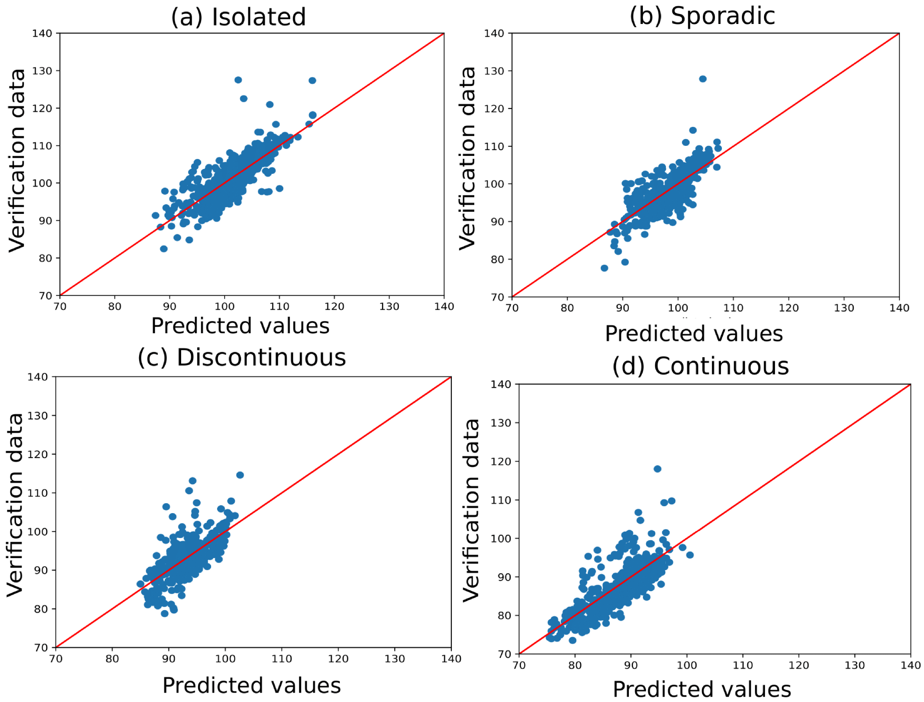

Figure 6. Predicted (x-axis, using Equation (1) with coefficients from Table 2) versus observed (y-axis) onset of surface freeze-back (counted from 1 July) for (**a**) isolated, (**b**) sporadic, (**c**) discontinuous, and (**d**) continuous permafrost zones in the study area. These scatterplots are based on the 10% of the data that was not used for training of the spatial regression model.

4. Discussion

4.1. Surface Freeze-Back Delayed but Not Equally Across Permafrost Zones

Our results indicate that the factors controlling the onset of surface freeze-back in permafrost regions vary significantly across space. While treating the entire study area as a single unit yields more accurate predictions (in a statistical sense), subdividing by permafrost zone reveals important differences in the influence of individual controls. For instance, vegetation emerges as a significant predictor in the isolated, sporadic, and discontinuous zones, but not in the continuous permafrost zone (Table 2).

Freeze-back also occurs at different times of the year across permafrost types, with the earliest onset observed in the continuous permafrost zone (Figure 4 and Figure A2 from Appendix A). Between 1950 and 2020, the onset of surface freeze-back was delayed by approximately three days in continuous permafrost areas, compared to a 5-day delay in the discontinuous, sporadic, and isolated zones (Figure 4).

In the context of ongoing Arctic climate change and Arctic amplification, these findings suggest that ground temperature responses to key predictors of freeze-back onset evolve more rapidly in thermally marginal permafrost zones (discontinuous, sporadic, and isolated), while continuous permafrost shows a more limited shift (for now).

At high latitudes where permafrost is predominantly continuous (Figure 2), persistent winds are a well-documented feature of the environment [64–66]. These strong winds contribute to highly variable snow distribution (in extent and depth), resulting in patchy snow cover across the landscape [67,68]. Because snow is a key control of ground temperature at the field scale, this spatial variability in snow cover translates into variability in the degree of insulation it provides, and ultimately the variability in the date of surface freeze-back. Given the strong local influence of snow on freeze-back timing, greater heterogeneity in snow cover likely leads to greater variability in the onset of surface freeze-back within the continuous permafrost zone. This spatial variability may help explain why the overall trend in freeze-back delay is weaker in continuous permafrost areas: in some locations, early freeze-back may offset later onset elsewhere, thereby dampening the overall trend signal for that permafrost zone.

4.2. Limitations of the Study

ERA5-Land has been shown to exhibit a warm bias in high-latitude permafrost regions, particularly during winter months [27] with the strongest overestimations over Canada and Alaska. The biases over Siberia are less pronounced but regionally evident. The period analyzed in this study (July to November) is associated with smaller biases than those observed in winter. For verification, a comparison between ERA5-Land and representative station data has been conducted to verify that ERA5-Land captures the first-order seasonality and thermal regime variability for the temperature in the upper soil layer (Figure A3 from Appendix A). While a systematic temperature bias in ERA5-Land could affect both the estimated onset of surface freeze-back and the predictor variables used in the regression, such a bias would primarily influence absolute values—not temporal trends—assuming that this bias is, of course, stationary in time. Therefore, while the exact dates of surface freeze-back should not be taken at face value, the trends and spatial relationships identified in this study remain robust. Also, for data processing reasons, we have used a twice-daily sampling as a proxy for the daily mean, which could slightly affect the result if the diurnal cycle is skewed. Finally, we acknowledge that the analyses presented here are based on a reanalysis product which is derived from a model, and that the relationships found could partly reflect inter-variable modeled relationships and not necessarily real-world relationships.

At the field scale (~meters), snow cover and vegetation are widely recognized as the primary factors influencing ground temperature, largely due to their insulating properties [38,55,69–71]. These factors can also be monitored via remote sensing, using indicators such as land surface temperature, snow cover, and vegetation indices [72,73]. At first glance, these findings may seem to contrast with our results, where snow cover emerges as a secondary predictor after air temperature, and vegetation shows a significant impact only when the analysis is delineated by permafrost zone. Nevertheless, we acknowledge that the permafrost zonation itself may have evolved over the study period. This apparent discrepancy may partly arise from the overrepresentation of continuous permafrost in our study area, where vegetation has little variability and is not a significant predictor. More fundamentally, the difference in spatial scale likely plays a major role. At the coarser resolution of ERA5-Land (~9 km), fine-scale heterogeneity in snow and vegetation is not fully captured, which may diminish their statistical influence on the freeze-back date. Additionally, the importance of surface temperature in our model results may indirectly reflect sub-grid variability in snow cover and vegetation, so that surface temperature would in fact act as a proxy for these unresolved processes.

4.3. Implications for Permafrost and Seasonally Frozen Regions

A delayed onset of surface freeze-back extends the window of favorable conditions for vegetation growth, potentially contributing to the observed Arctic greening [74]. In turn, increased vegetation productivity or changes in vegetation cover [75,76] can further influence the timing of surface freeze-back. Recent studies have highlighted the complexity of vegetation–soil interactions in permafrost regions, particularly the extension of the late root growing season prior to the complete freezing of the surface soil layer [77]. During this period, plants may access deeper mineral layers, promoting root development and altering nutrient cycling [78–80]. These dynamics can drive differential vegetation responses, such as increased root biomass—enhancing soil carbon storage—or even shifts in species composition [79]. Such changes are further amplified by modifications in the hydrological regimes, which often accompany permafrost degradation [78]. Altogether, shifts in freeze-back timing can trigger cascading, long-term consequences that extend beyond the growing season. These include broader impacts on surface albedo, soil structure, and ground stability—factors with important implications for infrastructure [81–83] and Arctic ecosystem functioning and feedback to the climate system.

There are still large uncertainties regarding whether Arctic landscapes will become wetter or drier in the future, particularly at regional scales [84]. This uncertainty has major implications for vegetation changes in the Arctic. In drier conditions, vegetation is expected to become shrub-dominated [34,85,86]. Increased shrub cover, in turn, would enhance snow interception [39,87] thereby altering the thermal insulation provided by snow and influencing the timing of surface freeze-back. These interactions are further complicated by feedback between snow cover and vegetation dynamics, making the system's evolution highly nonlinear. Establishing a robust present-day baseline for the timing and controls of surface freeze-back was therefore a key objective of this study, providing a reference point for future modeling.

A delayed onset of surface freeze-back also favors microbial activity, thereby contributing to permafrost-derived CO_2 and CH_4 emissions [88]. Although the majority of CH_4 emissions occur during the thawing season, approximately 14% of the mean annual CH_4 flux is released between the onset of surface freeze-back and the complete refreezing of the active layer [17].

During the transitional period between the onset of surface freeze-back and the complete refreezing of the active layer, parts of the soil remain unfrozen and biologically active, allowing continued microbial processes [89]. Extending the window for soil biogeochemical activity during the late shoulder season—bridging the thawing and freezing periods—is also critical for the mobilization and export of dissolved organic carbon (DOC) from soils [57,90]. Once exported to aquatic systems, this DOC becomes susceptible to microbial and photodegradation, altering the fate and persistence of carbon in the Arctic environment [91].

4.4. Outlook

This study is primarily diagnostic, based on linear relationships established between predictor and predictand variables. However, it can serve as a foundation for predictive applications of the onset of surface freeze-back. Many weather and climate centers routinely publish seasonal forecasts of variables such as precipitation and near-surface air temperature. These forecasts, when combined and downscaled with the regression models developed in this work, could be used to produce probabilistic estimates of freeze-back onset with a lead time of several days to weeks. Although such estimates would carry uncertainties stemming from the forecast inputs, they could provide valuable information for logistical planning of field campaigns in permafrost regions. Moreover, timely knowledge of freeze-back onset could help constrain land surface models and improve representation of cold-season processes.

The predictors used in this model—air temperature, snow cover, and vegetation—are included in seasonal forecast systems, such as those from the European Center for Medium-Range Weather Forecasts (ECMWF), making them available several months in advance. These forecasts could be used to generate probability distributions of expected freeze-back dates under current and near-future climate conditions.

Looking ahead, understanding how these key variables are projected to change can offer insights into future trends in the onset of surface freeze-back. While air temperature, snow cover, and vegetation are all expected to evolve under climate change, their trajectories will be spatially heterogeneous [92,93]. This suggests that future changes in freeze-back timing—and the associated permafrost carbon emissions—will also vary regionally, underlining the importance of spatially explicit projections.

5. Conclusions

The primary objective of this study was to document large-scale temporal changes in the onset of surface freeze-back across Siberian permafrost regions. Over the 70-year period from 1950 to 2020, the average onset of surface freeze-back (defined at 0–7 cm of soil depth) over a 4.2 million km^2 area in Siberia (45–65° N, 95–125° E) has shifted by approximately five days—delaying from 12 October to 17 October.

We also investigated the environmental controls of this shift using a spatial error model, a type of spatial regression that accounts for spatial autocorrelation in the residuals. We acknowledge that the correlation matrix and variance inflation factor (VIF) for the predictors, which are usual tools to detect possible collinearity in the predictors, are not explored in this study. One of the main findings is that, at the coarse spatial scale of ERA5-Land (~0.1° resolution), near-surface air temperature is the variable most closely associated with surface freeze-back onset, followed by snow cover. This result contrasts with numerous field studies, which emphasize the roles of snow and vegetation as primary controls. This apparent discrepancy likely arises from scale differences: field studies can resolve fine-scale processes (e.g., snow interception, microtopography, vegetation heterogeneity) that are smoothed out at the coarse scale used here.

The spatial regression model was applied to both the full study area and to subsets defined by permafrost zone. While the model applied to the entire domain yielded the highest statistical predictive accuracy (R^2 = 0.78), stratifying the analysis by permafrost zone provided deeper insight into how the influence of distinct environmental variables varies with permafrost type. In particular, while air temperature and snow insulation timing remained significant across all zones, vegetation insulation was found to be only significantly linked to the timing of freeze-back in the discontinuous, sporadic, and isolated permafrost zones, but not in the continuous permafrost zone. This supports the idea that the influence of vegetation on the seasonality of freeze-back is more pronounced in thermally marginal permafrost environments.

Overall, our results highlight the dominant role of air temperature in controlling freeze-back timing at large scales, with snow cover and vegetation playing secondary but still important roles. These findings reflect both the resolution of the dataset and the interdependence of variables at this scale. More broadly, they highlight how the choice of spatial scale can shape our understanding of permafrost processes. Large-scale diagnostics, such as the one presented here, complement fine-scale studies by providing an integrated perspective on regional patterns and controls.

Author Contributions: Conceptualization, C.O., S.O. and F.M.; methodology, C.O., S.O., A.D. and F.M.; investigation, C.O.; data curation, C.O.; writing—review and editing, C.O., S.O., A.D. and F.M.; visualization, C.O. and F.M.; supervision, S.O. and F.M. All authors have read and agreed to the published version of the manuscript.

Funding: This research was funded by the Belgian Science Policy Office (BELSPO) under the RESIST project (contract no. RT/23/RESIST), by the Fédération Wallonie Bruxelles (FWB) Cellule Europe at UCLouvain, and by a Fonds Spécial de Recherches (FSR) at UCLouvain.

Institutional Review Board Statement: Not applicable.

Informed Consent Statement: Not applicable.

Data Availability Statement: The original data presented in the study are openly available at https://doi.org/10.5281/zenodo.14832934, https://cds.climate.copernicus.eu/datasets/reanalysis-era5-land?tab=overview, https://forobs.jrc.ec.europa.eu/glc2000, (accessed on 10 October 2024) and https://doi.org/10.1594/PANGAEA.888600.

Acknowledgments: Cécile Osy is supported by an incentive from the Fédération Wallonie Bruxelles. François Massonnet is a F.R.S.–FNRS Research Associate, and Sophie Opfergelt is a F.R.S.–FNRS Senior Research Associate.

Conflicts of Interest: The authors declare no conflicts of interest.

Appendix A

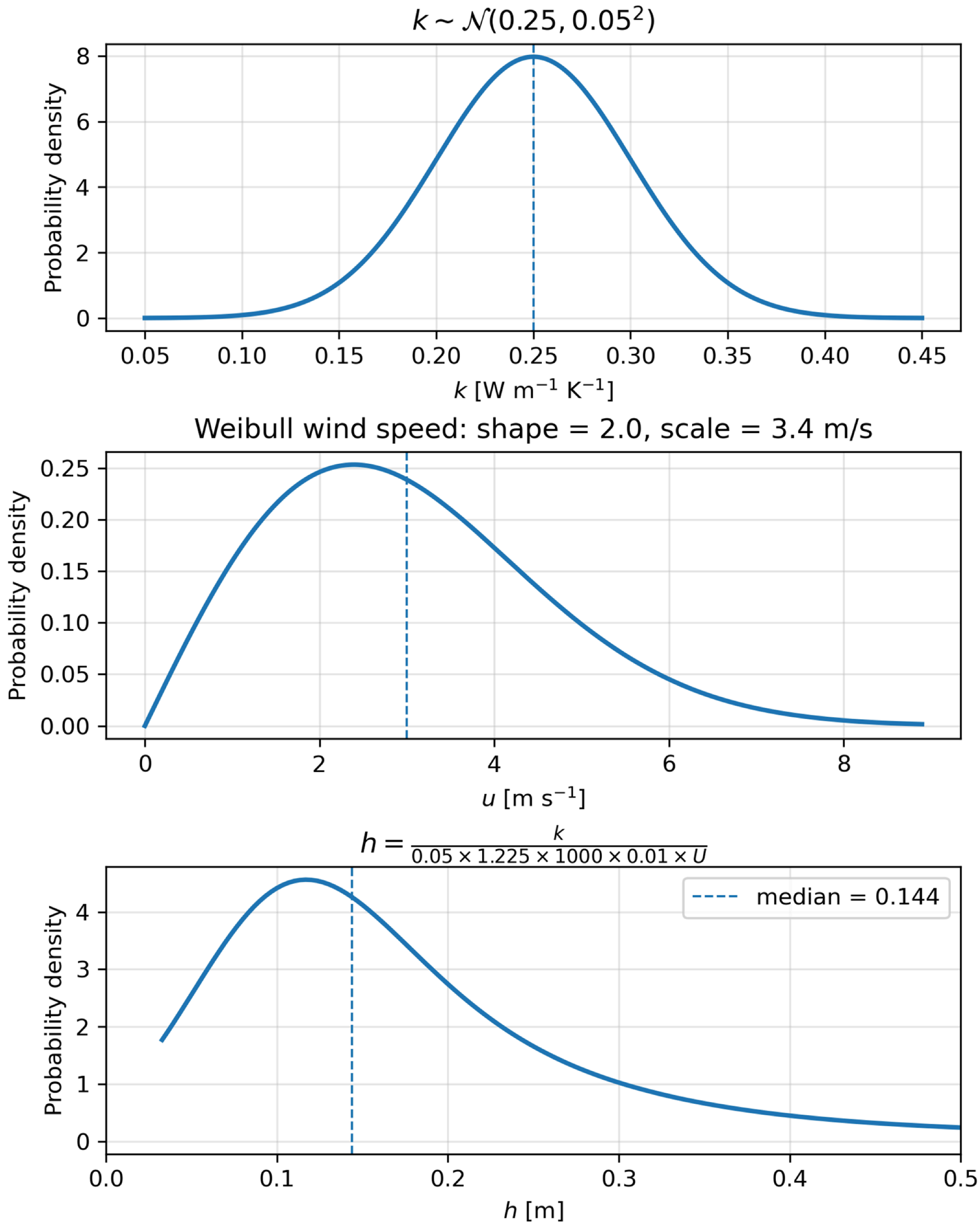

Figure A1. Distribution of critical snow thickness (bottom panel) for which insulation reduces the no-snow land-to-atmosphere heat flux by 95%, as a function of assumed distributions of snow conductivity (top panel) and wind speed (middle panel). These two distributions have been chosen so that their expectation matches the values used in the main text.

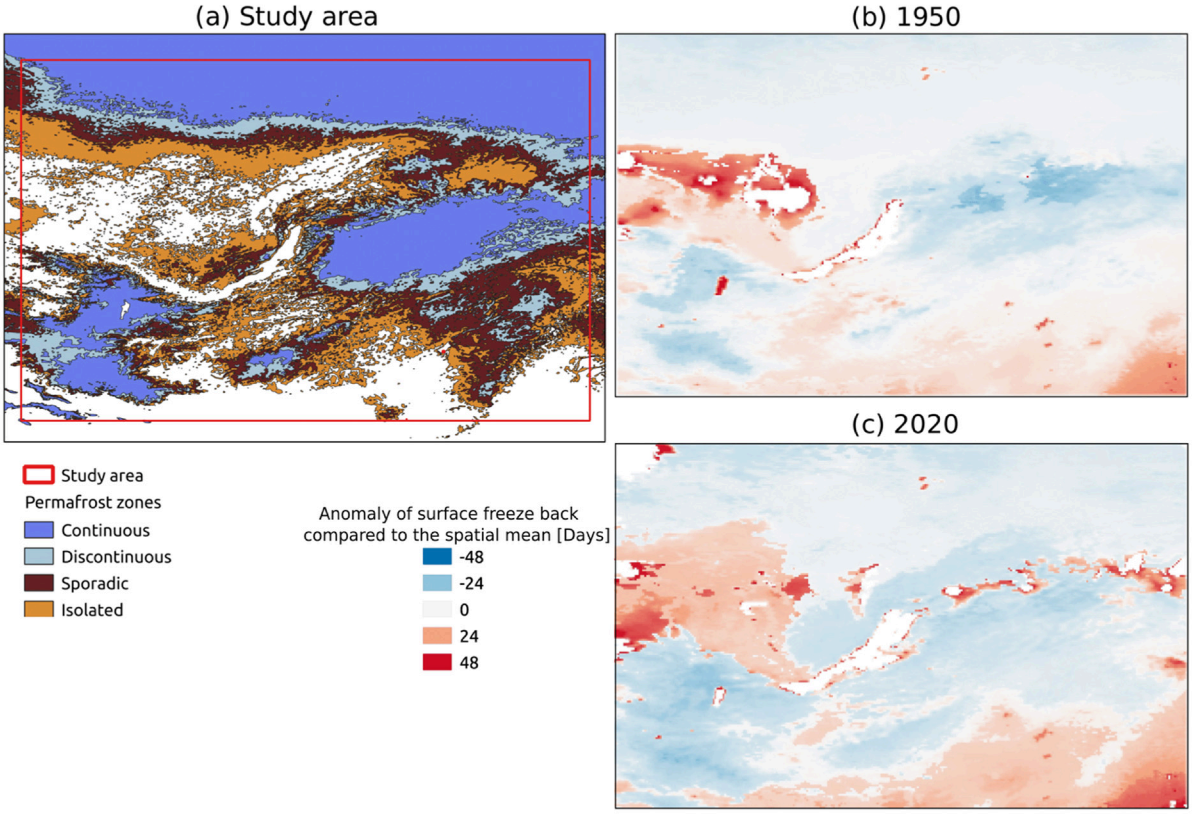

Figure A2. Study area (**a**) and spatial variation in the anomaly of the onset of the surface freeze-back relative to the spatial average for (**b**) the first year of the study (1950) and (**c**) the last year of the study (2020). Red areas mean that surface freeze-back occurs later than the spatial average and blue areas mean that surface freeze-back occurs earlier than the spatial average.

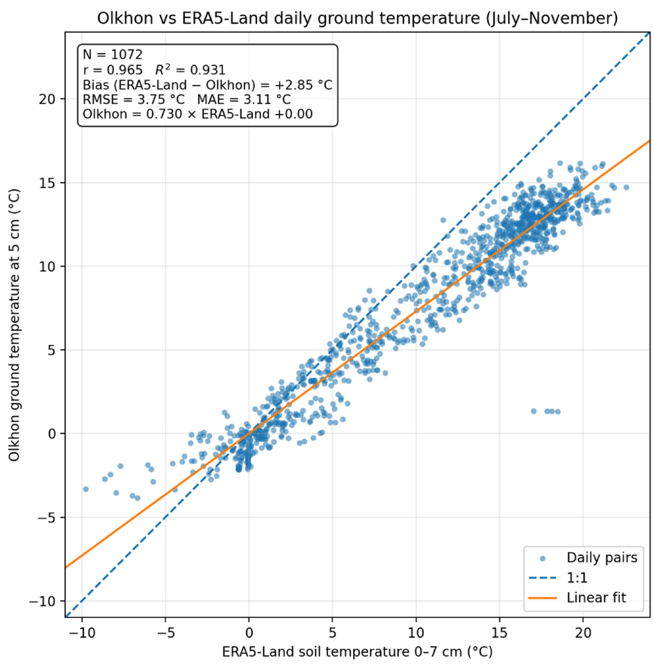

Figure A3. ERA5-Land 0–7 cm average soil temperature versus Global Terrestrial Network for Permafrost (GTN-P) data of temperature at 5 cm for the Olkhon Station (53.23032° N, 107.43966° E) between 2012 and 2019, for the months July to November only.

References

1. Obu, J. How Much of the Earth's Surface is Underlain by Permafrost? *J. Geophys. Res. Earth Surf.* **2021**, *126*, e2021JF006123. [CrossRef]
2. Zhang, T.; Heginbottom, J.A.; Barry, R.G.; Brown, J. Further statistics on the distribution of permafrost and ground ice in the Northern Hemisphere[1]. *Polar Geogr.* **2000**, *24*, 126–131. [CrossRef]
3. Canadell, J.G.; Monteiro, P.M.S.; Costa, M.H.; Cotrim, L.; Cunha, D.; Cox, P.M.; Eliseev, A.V.; Henson, S.; Ishii, M.; Jaccard, S.; et al. *2021: Global Carbon and Other Biogeochemical Cycles and Feedbacks In Climate Change 2021: The Physical Science Basis Contribution of Working Group I to the Sixth Assessment Report of the Intergovernmental Panel on Climate Change*; Masson-Delmotte, V., Zhai, P., Pirani, A., Connors, S.L., Péan, C., Berger, S., Caud, N., Chen, Y., Goldfarb, L., Gomis, M.I., et al., Eds.; Cambridge University Press: Cambridge, UK; New York, NY, USA, 2021; pp. 673–816.
4. Pithan, F.; Mauritsen, T. Arctic amplification dominated by temperature feedbacks in contemporary climate models. *Nat. Geosci.* **2014**, *7*, 181–184. [CrossRef]
5. Overland, J.E. Long-range linkage. *Nat. Clim. Change* **2014**, *4*, 11–12. [CrossRef]
6. Rantanen, M.; Karpechko, A.Y.; Lipponen, A.; Nordling, K.; Hyvärinen, O.; Ruosteenoja, K.; Vihma, T.; Laaksonen, A. The Arctic has warmed nearly four times faster than the globe since 1979. *Commun. Earth Environ.* **2022**, *3*, 168. [CrossRef]
7. Gulev, S.K.; Thorne, P.W.; Ahn, J.; Dentener, F.J.; Domingues, C.M.; Gerland, S.; Gong, D.; Kaufman, D.S.; Nnamchi, H.C.; Quaas, J.; et al. Changing State of the Climate System. In *Climate Change 2021: The Physical Science Basis*; Masson-Delmotte, V., Zhai, P., Pirani, A., Connors, S.L., Péan, C., Berger, S., et al., Eds.; Cambridge University Press: Cambridge, UK; New York, NY, USA, 2021; pp. 287–422. [CrossRef]
8. Intergovernmental Panel on Climate Change (IPCC). Summary for Policymakers. In *The Ocean and Cryosphere in a Changing Climate: Special Report of the Intergovernmental Panel on Climate Change*; Pörtner, H.-O., Roberts, D.C., Masson-Delmotte, V., Zhai, P., Tignor, M., Poloczanska, E., Mintenbeck, K., Alegría, A., Nicolai, M., Okem, A., et al., Eds.; Cambridge University Press: Cambridge, UK; New York, NY, USA, 2022; pp. 3–35. [CrossRef]
9. Peng, X.; Zhang, T.; Frauenfeld, O.W.; Mu, C.; Wang, K.; Wu, X.; Guo, D.; Luo, J.; Hjort, J.; Aalto, J.; et al. Active Layer Thickness and Permafrost Area Projections for the 21st Century. *Earth's Futur.* **2023**, *11*, e2023EF003573. [CrossRef]
10. Caretta, M.A.; Mukherji, A.; Arfanuzzaman, M.; Betts, R.A.; Gelfan, A.; Hirabayashi, Y.; Lissner, T.K.; Liu, J.; Lopez Gunn, E.; Morgan, R.; et al. 2022: Water. In *Climate Change 2022: Impacts, Adaptation and Vulnerability Contribution of Working Group II to the Sixth Assessment Report of the Intergovernmental Panel on Climate Change*; Pörtner, H.-O., Roberts, D.C., Tignor, M., Poloczanska, E.S., Mintenbeck, K., Alegría, A., Craig, M., Langsdorf, S., Löschke, S., Möller, V., et al., Eds.; Cambridge University Press: Cambridge, UK; New York, NY, USA, 2023; pp. 551–712. [CrossRef]
11. Schuur, E.A.G.; Bockheim, J.; Canadell, J.G.; Euskirchen, E.; Field, C.B.; Goryachkin, S.V.; Hagemann, S.; Kuhry, P.; LaFleur, P.M.; Lee, H.; et al. Vulnerability of Permafrost Carbon to Climate Change: Implications for the Global Carbon Cycle. *Bioscience* **2008**, *58*, 701–714. [CrossRef]
12. Schaefer, K.; Lantuit, H.; Romanovsky, V.E.; Schuur, E.A.G.; Witt, R. The Impact of the Permafrost Carbon Feedback on Global Climate. *Environ. Res. Lett.* **2014**, *9*, 085003. [CrossRef]
13. Schuur, E.A.G.; McGuire, A.; Romanovsky, V.E.; Schädel, C.; Mack, M. Second State of the Carbon Cycle Report (SOCCR2): A Sustained Assessment Report. In *Arctic and Boreal Carbon*; Chapter 11; US Global Change Research Program: Washington, DC, USA, 2018; pp. 428–468.
14. Nitzbon, J.; von Deimling, T.S.; Aliyeva, M.; Chadburn, S.E.; Grosse, G.; Laboor, S.; Lee, H.; Lohmann, G.; Steinert, N.J.; Stuenzi, S.M.; et al. No respite from permafrost-thaw impacts in the absence of a global tipping point. *Nat. Clim. Change* **2024**, *14*, 573–585. [CrossRef]
15. Elberling, B.; Brandt, K.K. Uncoupling of microbial CO_2 production and release in frozen soil and its implications for field studies of arctic C cycling. *Soil Biol. Biochem.* **2003**, *35*, 263–272. [CrossRef]
16. Miner, K.R.; Turetsky, M.R.; Malina, E.; Bartsch, A.; Tamminen, J.; McGuire, A.D.; Fix, A.; Sweeney, C.; Elder, C.D.; Miller, C.E. Permafrost carbon emissions in a changing Arctic. *Nat. Rev. Earth Environ.* **2022**, *3*, 55–67. [CrossRef]
17. Rößger, N.; Sachs, T.; Wille, C.; Boike, J.; Kutzbach, L. Seasonal increase of methane emissions linked to warming in Siberian tundra. *Nat. Clim. Change* **2022**, *12*, 1031–1036. [CrossRef]
18. Huang, J.; Zhang, X.; Zhang, Q.; Lin, Y.; Hao, M.; Luo, Y.; Zhao, Z.; Yao, Y.; Chen, X.; Wang, L.; et al. Recently amplified arctic warming has contributed to a continual global warming trend. *Nat. Clim. Change* **2017**, *7*, 875–879. [CrossRef]
19. Siewert, M.B.; Lantuit, H.; Richter, A.; Hugelius, G. Permafrost Causes Unique Fine-Scale Spatial Variability Across Tundra Soils. *Glob. Biogeochem. Cycles* **2021**, *35*, e2020GB006659. [CrossRef]
20. Shogren, A.J.; Zarnetske, J.P.; Abbott, B.W.; Iannucci, F.; Bowden, W.B. We cannot shrug off the shoulder seasons: Addressing knowledge and data gaps in an Arctic headwater. *Environ. Res. Lett.* **2020**, *15*, 104027. [CrossRef]
21. Romanovsky, V.; Sazonova, T.; Balobaev, V.; Shender, N.; Sergueev, D. Past and recent changes in air and permafrost temperatures in eastern Siberia. *Glob. Planet. Change* **2007**, *56*, 399–413. [CrossRef]

22. Batir, J.F.; Hornbach, M.J.; Blackwell, D.D. Ten years of measurements and modeling of soil temperature changes and their effects on permafrost in Northwestern Alaska. *Glob. Planet. Change* **2017**, *148*, 55–71. [CrossRef]
23. Smith, S.L.; O'neill, H.B.; Isaksen, K.; Noetzli, J.; Romanovsky, V.E. The changing thermal state of permafrost. *Nat. Rev. Earth Environ.* **2022**, *3*, 10–23. [CrossRef]
24. Obu, J.; Westermann, S.; Kääb, A.; Bartsch, A. *Ground Temperature Map, 2000–2016, Northern Hemisphere Permafrost*; Pangaea Type: Dataset; Alfred Wegener Institute, Helmholtz Centre for Polar and Marine Research: Bremerhaven, Germany, 2018.
25. Muñoz-Sabater, J.; Dutra, E.; Agustí-Panareda, A.; Albergel, C.; Arduini, G.; Balsamo, G.; Boussetta, S.; Choulga, M.; Harrigan, S.; Hersbach, H.; et al. ERA5-Land: A state-of-the-art global reanalysis dataset for land applications. *Earth Syst. Sci. Data Discuss.* **2021**, *13*, 4349–4383. [CrossRef]
26. Hersbach, H.; Bell, B.; Berrisford, P.; Hirahara, S.; Horányi, A.; Muñoz-Sabater, J.; Nicolas, J.; Peubey, C.; Radu, R.; Schepers, D.; et al. The ERA5 global reanalysis. *Q. J. R. Meteorol. Soc.* **2020**, *146*, 1999–2049. [CrossRef]
27. Cao, B.; Gruber, S.; Zheng, D.; Li, X. The ERA5-Land soil temperature bias in permafrost regions. *Cryosphere* **2020**, *14*, 2581–2595. [CrossRef]
28. Torre, D.D.; Di Marco, N.; Menapace, A.; Avesani, D.; Righetti, M.; Majone, B. Suitability of ERA5-Land reanalysis dataset for hydrological modelling in the Alpine region. *J. Hydrol. Reg. Stud.* **2024**, *52*, 101718. [CrossRef]
29. Lesage, J.; Pace, R.K. *Introduction to Spatial Econometrics*; Chapman and Hall/CRC Press: Boca Raton, FL, USA, 2009. [CrossRef]
30. Breusch, T.S.; Pagan, A.R. The Lagrange Multiplier Test and its Applications to Model Specification in Econometrics. *Rev. Econ. Stud.* **1980**, *47*, 239–253. [CrossRef]
31. Beck, P.S.A.; Goetz, S.J. Satellite observations of high northern latitude vegetation productivity changes between 1982 and 2008: Ecological variability and regional differences. *Environ. Res. Lett.* **2011**, *6*, 045501. [CrossRef]
32. Billings, W.D. Constraints to Plant Growth, Reproduction, and Establishment in Arctic Environments. *Arct. Alp. Res.* **1987**, *19*, 357–365. [CrossRef]
33. Rixen, C.; Wipf, S.; Frei, E.; Stöckli, V. Faster, higher, more? Past, present and future dynamics of alpine and arctic flora under climate change. *Alp. Bot.* **2014**, *124*, 77–79. [CrossRef]
34. Heijmans, M.M.P.D.; Magnússon, R.Í.; Lara, M.J.; Frost, G.V.; Myers-Smith, I.H.; van Huissteden, J.; Jorgenson, M.T.; Fedorov, A.N.; Epstein, H.E.; Lawrence, D.M.; et al. Tundra vegetation change and impacts on permafrost. *Nat. Rev. Earth Environ.* **2022**, *3*, 68–84. [CrossRef]
35. Aalto, J.; le Roux, P.C.; Luoto, M. Vegetation Mediates Soil Temperature and Moisture in Arctic-Alpine Environments. *Arct. Antarct. Alp. Res.* **2013**, *45*, 429–439. [CrossRef]
36. Ehrenfeld, J.G.; Ravit, B.; Elgersma, K. Feedback in the plant-soil system. *Annu. Rev. Environ. Resour.* **2005**, *30*, 75–115. [CrossRef]
37. Asbjornsen, H.; Goldsmith, G.R.; Alvarado-Barrientos, M.S.; Rebel, K.; Van Osch, F.P.; Rietkerk, M.; Chen, J.; Gotsch, S.; Tobón, C.; Geissert, D.R.; et al. Ecohydrological advances and applications in plant-water relations research: A review. *J. Plant Ecol.* **2011**, *4*, 3–22. [CrossRef]
38. Kropp, H.; Loranty, M.M.; Natali, S.M.; Kholodov, A.L.; Rocha, A.V.; Myers-Smith, I.H.; Abbott, B.W.; Abermann, J.; Blanc-Betes, E.; Blok, D.; et al. Shallow soils are warmer under trees and tall shrubs across Arctic and Boreal ecosystems. *Environ. Res. Lett.* **2020**, *16*, 015001. [CrossRef]
39. Sturm, M.; Racine, C.; Tape, K. Increasing shrub abundance in the Arctic. *Nature* **2001**, *411*, 546–547. [CrossRef] [PubMed]
40. Schuur, E.A.G.; McGuire, A.D.; Schädel, C.; Grosse, G.; Harden, J.W.; Hayes, D.J.; Hugelius, G.; Koven, C.D.; Kuhry, P.; Lawrence, D.M.; et al. Climate change and the permafrost carbon feedback. *Nature* **2015**, *520*, 171–179. [CrossRef] [PubMed]
41. Wang, Z.; Kim, Y.; Seo, H.; Um, M.-J.; Mao, J. Permafrost response to vegetation greenness variation in the Arctic tundra through positive feedback in surface air temperature and snow cover. *Environ. Res. Lett.* **2019**, *14*, 044024. [CrossRef]
42. Druel, A.; Peylin, P.; Krinner, G.; Ciais, P.; Viovy, N.; Peregon, A.; Bastrikov, V.; Kosykh, N.; Mironycheva-Tokareva, N. Towards a more detailed representation of high-latitude vegetation in the global land surface model ORCHIDEE (ORC-HL-VEGv1.0). *Geosci. Model Dev.* **2017**, *10*, 4693–4722. [CrossRef]
43. Mamet, S.D.; Chun, K.P.; Kershaw, G.G.L.; Loranty, M.M.; Kershaw, G.P. Recent Increases in Permafrost Thaw Rates and Areal Loss of Palsas in the Western Northwest Territories, Canada. *Permafr. Periglac. Process.* **2017**, *28*, 619–633. [CrossRef]
44. Paradis, M.; Lévesque, E.; Boudreau, S. Greater effect of increasing shrub height on winter versus summer soil temperature. *Environ. Res. Lett.* **2016**, *11*, 085005. [CrossRef]
45. Wynn, T.M.; Mostaghimi, S. Effects of riparian vegetation on stream bank subaerial processes in southwestern Virginia, USA. *Earth Surf. Process. Landf.* **2006**, *31*, 399–413. [CrossRef]
46. Wu, J.-H.; Tang, C.-S.; Shi, B.; Gao, L.; Jiang, H.-T.; Daniels, J.L. Effect of Ground Covers on Soil Temperature in Urban and Rural Areas. *Environ. Eng. Geosci.* **2014**, *20*, 225–237. [CrossRef]
47. Forbes, B.C.; Fauria, M.M.; Zetterberg, P. Russian Arctic warming and 'greening' are closely tracked by tundra shrub willows. *Glob. Change Biol.* **2010**, *16*, 1542–1554. [CrossRef]

48. Myers-Smith, I.H.; Kerby, J.T.; Phoenix, G.K.; Bjerke, J.W.; Epstein, H.E.; Assmann, J.J.; John, C.; Andreu-Hayles, L.; Angers-Blondin, S.; Beck, P.S.A.; et al. Complexity revealed in the greening of the Arctic. *Nat. Clim. Change* **2020**, *10*, 106–117. [CrossRef]
49. Lawrence, D.M.; Koven, C.D.; Swenson, S.C.; Riley, W.J.; Slater, A.G. Permafrost thaw and resulting soil moisture changes regulate projected high-latitude CO_2 and CH_4 emissions. *Environ. Res. Lett.* **2015**, *10*, 094011. [CrossRef]
50. Ye, B.; Yang, D.; Zhang, Z.; Kane, D.L. Variation of hydrological regime with permafrost coverage over Lena Basin in Siberia. *J. Geophys. Res.* **2009**, *114*, D07102. [CrossRef]
51. Walvoord, M.A.; Kurylyk, B.L. Hydrologic Impacts of Thawing Permafrost—A Review. *Vadose Zone J.* **2016**, *15*, 1–20. [CrossRef]
52. Smith, S.L.; Riseborough, D.W.; Bonnaventure, P.P.; Duchesne, C. An ecoregional assessment of freezing season air and ground surface temperature in the Mackenzie Valley corridor, NWT, Canada. *Cold Reg. Sci. Technol.* **2016**, *125*, 152–161. [CrossRef]
53. Morse, P.; Burn, C.; Kokelj, S. Influence of snow on near-surface ground temperatures in upland and alluvial environments of the outer Mackenzie Delta, Northwest Territories. *Can. J. Earth Sci.* **2012**, *49*, 895–913. [CrossRef]
54. Peng, X.; Zhang, T.; Frauenfeld, O.W.; Wang, K.; Cao, B.; Zhong, X.; Su, H.; Mu, C. Response of seasonal soil freeze depth to climate change across China. *Cryosphere* **2017**, *11*, 1059–1073. [CrossRef]
55. Zhang, T. Influence of the seasonal snow cover on the ground thermal regime: An overview. *Rev. Geophys.* **2005**, *43*. [CrossRef]
56. Yen, Y. *Review of Thermal Properties of Snow, Ice and Sea Ice*; Report 81-10; US Army Cold Regions Research and Engineering Laboratory: Hanover, NH, USA, 1981.
57. Villani, M.; Hirst, C.; D'alsche, E.d.B.; Thomas, M.; Lundin, E.; Giesler, R.; Mörth, C.-M.; Opfergelt, S. Lengthening of biogeochemical processes during winter in degraded permafrost soils. *Geochem. Perspect. Lett.* **2025**, *34*, 36–42. [CrossRef]
58. Lafrenière, M.J.; Laurin, E.; Lamoureux, S.F. The Impact of Snow Accumulation on the Active Layer Thermal Regime in High Arctic Soils. *Vadose Zone J.* **2013**, *12*, 1–13. [CrossRef]
59. Chavez-Chong, C. Cross-Validation for Spatial Data. 2024. Available online: https://hal.science/hal-04605503v1 (accessed on 10 October 2024).
60. Osterkamp, T.E.; Jorgenson, M.T.; Schuur, E.A.G.; Shur, Y.L.; Kanevskiy, M.Z.; Vogel, J.G.; Tumskoy, V.E. Physical and ecological changes associated with warming permafrost and thermokarst in Interior Alaska. *Permafr. Periglac. Process.* **2009**, *20*, 235–256. [CrossRef]
61. Del Vecchio, J.; Evans, S.G. Climate and Hydrogeological Controls on Water Tracks in Permafrost Landscapes. *Rev. Geophys.* **2025**, *63*, e2024RG000854. [CrossRef]
62. Rodenhizer, H.; Belshe, F.; Celis, G.; Ledman, J.; Mauritz, M.; Goetz, S.; Sankey, T.; Schuur, E.A. Abrupt permafrost thaw accelerates carbon dioxide and methane release at a tussock tundra site. *Arct. Antarct. Alp. Res.* **2022**, *54*, 443–464. [CrossRef]
63. McDonnell, J.J.; Spence, C.; Karran, D.J.; van Meerveld, H.J.I.; Harman, C.J. Fill-and-Spill: A Process Description of Runoff Generation at the Scale of the Beholder. *Water Resour. Res.* **2021**, *57*, e2020WR027514. [CrossRef]
64. Wilson, J.W. Notes on Wind and its Effects in Arctic-Alpine Vegetation. *J. Ecol.* **1959**, *47*, 415. [CrossRef]
65. Sturm, M.; Liston, G.E.; Benson, C.S.; Holmgren, J. Characteristics and Growth of a Snowdrift in Arctic Alaska, U.S.A. *Arct. Antarct. Alp. Res.* **2001**, *33*, 319–329. [CrossRef]
66. Gisnås, K.; Westermann, S.; Schuler, T.V.; Melvold, K.; Etzelmüller, B. Small-Scale Variation of Snow in a Regional Permafrost Model. *Cryosphere* **2016**, *10*, 1201–1215. [CrossRef]
67. Aas, K.S.; Gisnås, K.; Westermann, S.; Berntsen, T.K. A Tiling Approach to Represent Subgrid Snow Variability in Coupled Land Surface–Atmosphere Models. *J. Hydrometeorol.* **2017**, *18*, 49–63. [CrossRef]
68. Gisnås, K.; Westermann, S.; Schuler, T.V.; Litherland, T.; Isaksen, K.; Boike, J.; Etzelmüller, B. A statistical approach to represent small-scale variability of permafrost temperatures due to snow cover. *Cryosphere* **2014**, *8*, 2063–2074. [CrossRef]
69. Luetschg, M.; Stoeckli, V.; Lehning, M.; Haeberli, W.; Ammann, W. Temperatures in two boreholes at Flüela Pass, Eastern Swiss Alps: The effect of snow redistribution on permafrost distribution patterns in high mountain areas. *Permafr. Periglac. Process.* **2004**, *15*, 283–297. [CrossRef]
70. Zhang, T.; Barry, R.G.; Haeberli, W. Numerical simulations of the influence of the seasonal snow cover on the occurrence of permafrost at high latitudes. *Nor. Geogr. Tidsskr. Nor. J. Geogr.* **2001**, *55*, 261–266. [CrossRef]
71. Loranty, M.M.; Abbott, B.W.; Blok, D.; Douglas, T.A.; Epstein, H.E.; Forbes, B.C.; Jones, B.M.; Kholodov, A.L.; Kropp, H.; Malhotra, A.; et al. Reviews and syntheses: Changing ecosystem influences on soil thermal regimes in northern high-latitude permafrost regions. *Biogeosciences* **2018**, *15*, 5287–5313. [CrossRef]
72. Ylönen, M.; Marttila, H.; Geissler, J.; Kuzmin, A.; Korpelainen, P.; Kumpula, T.; Ala-Aho, P. UAV LiDAR surveys and machine learning improve snow depth and water equivalent estimates in boreal landscapes. *Cryosphere* **2025**, *19*, 4585–4610. [CrossRef]
73. Alphonse, A.B.; Osuch, M.; Wawrzyniak, T.; Hanselmann, N. Spatio-temporal variability of surface temperatures in High Arctic periglacial environment using UAV thermal imagery and in-situ measurements. *GISci. Remote Sens.* **2024**, *61*, 2435851. [CrossRef]
74. A Arndt, K.; Santos, M.J.; Ustin, S.; Davidson, S.J.; Stow, D.; Oechel, W.C.; Tran, T.T.P.; Graybill, B.; Zona, D. Arctic greening associated with lengthening growing seasons in Northern Alaska. *Environ. Res. Lett.* **2019**, *14*, 125018. [CrossRef]

75. Anderson, J.E.; Douglas, T.A.; Barbato, R.A.; Saari, S.; Edwards, J.D.; Jones, R.M. Linking vegetation cover and seasonal thaw depths in interior Alaska permafrost terrains using remote sensing. *Remote Sens. Environ.* **2019**, *233*, 111363. [CrossRef]
76. Druel, A.; Ciais, P.; Krinner, G.; Peylin, P. Modeling the Vegetation Dynamics of Northern Shrubs and Mosses in the ORCHIDEE Land Surface Model. *J. Adv. Model. Earth Syst.* **2019**, *11*, 2020–2035. [CrossRef]
77. Blume-Werry, G.; Milbau, A.; Teuber, L.M.; Johansson, M.; Dorrepaal, E. Dwelling in the deep—Strongly increased root growth and rooting depth enhance plant interactions with thawing permafrost soil. *New Phytol.* **2019**, *223*, 1328–1339. [CrossRef] [PubMed]
78. Finger, R.A.; Turetsky, M.R.; Kielland, K.; Ruess, R.W.; Mack, M.C.; Euskirchen, E.S. Effects of permafrost thaw on nitrogen availability and plant–soil interactions in a boreal Alaskan lowland. *J. Ecol.* **2016**, *104*, 1542–1554. [CrossRef]
79. Hewitt, R.E.; Taylor, D.L.; Genet, H.; McGuire, A.D.; Mack, M.C. Below-ground plant traits influence tundra plant acquisition of newly thawed permafrost nitrogen. *J. Ecol.* **2019**, *107*, 950–962. [CrossRef]
80. Ogden, E.L.; Cumming, S.G.; Smith, S.L.; Turetsky, M.R.; Baltzer, J.L. Permafrost thaw induces short-term increase in vegetation productivity in northwestern Canada. *Glob. Change Biol.* **2023**, *29*, 5352–5366. [CrossRef] [PubMed]
81. Zhou, X.; Su, Y.; Cheng, Y.; Li, Q. Preliminary Insight into Ice Melting, Surface Subsidence, and Wellhead Instability during Oil and Gas Extraction in Permafrost Region. *Energies* **2024**, *17*, 1292. [CrossRef]
82. Zhou, X.; Su, Y.; Cheng, Y.; Li, Q. Evaluation of Thermal Insulation of Vacuum-Insulated Casing to Prevent Uncontrollable Melting of Ice and Borehole Instability in Permafrost. *Processes* **2024**, *12*, 1389. [CrossRef]
83. Burn, C.R.; Bartsch, A.; Chakraborty, E.; Das, S.; Frauenfelder, R.; Gärtner-Roer, I.; Gisnås, K.G.; Herring, T.; Jones, B.M.; Kokelj, S.V.; et al. Developments in Permafrost Science and Engineering in Response to Climate Warming in Circumpolar and High Mountain Regions, 2019–2024. *Permafr. Periglac. Process.* **2025**, *36*, 167–188. [CrossRef]
84. Xie, S.-P.; Deser, C.; Vecchi, G.A.; Collins, M.; Delworth, T.L.; Hall, A.; Hawkins, E.; Johnson, N.C.; Cassou, C.; Giannini, A.; et al. Towards predictive understanding of regional climate change. *Nat. Clim. Change* **2015**, *5*, 921–930. [CrossRef]
85. Jónsdóttir, I.S.; Khitun, O.; Stenström, A. Biomass and nutrient responses of a clonal tundra sedge to climate warming. *Can. J. Bot.* **2005**, *83*, 1608–1621. [CrossRef]
86. Shaver, G.R.; Bret-Harte, M.S.; Jones, M.H.; Johnstone, J.; Gough, L.; Laundre, J.; Chapin, F.S. Species Composition Interacts with Fertilizer to Control Long-Term Change in Tundra Productivity. *Ecology* **2001**, *82*, 3163–3181. [CrossRef]
87. Chapin, F.S.; Iii, F.S.C.; Sturm, M.; Serreze, M.C.; McFadden, J.P.; Key, J.R.; Lloyd, A.H.; McGuire, A.D.; Rupp, T.S.; Lynch, A.H.; et al. Role of Land-Surface Changes in Arctic Summer Warming. *Science* **2005**, *310*, 657–660. [CrossRef] [PubMed]
88. Zona, D. Long-term effects of permafrost thaw. *Nature* **2016**, *537*, 625–626. [CrossRef] [PubMed]
89. Commane, R.; Lindaas, J.; Benmergui, J.; Luus, K.A.; Chang, R.Y.-W.; Daube, B.C.; Euskirchen, E.S.; Henderson, J.M.; Karion, A.; Miller, J.B.; et al. Carbon dioxide sources from Alaska driven by increasing early winter respiration from Arctic tundra. *Proc. Natl. Acad. Sci. USA* **2017**, *114*, 5361–5366. [CrossRef] [PubMed]
90. du Bois d'Aische, E.; Jonard, F.; Hirst, C.; Villani, M.; Thomas, M.; Giesler, R.; Mörth, C.-M.; Lundin, E.; Van Oost, K.; Vanacker, V.; et al. Permafrost thaw drives iron and organic carbon release into soil pore water during palsa to degraded palsa transition. *Permafr. Periglac. Process.* **2026**, *37*, 107–123. [CrossRef]
91. Bowen, J.C.; Ward, C.P.; Kling, G.W.; Cory, R.M. Arctic Amplification of Global Warming Strengthened by Sunlight Oxidation of Permafrost Carbon to CO_2. *Geophys. Res. Lett.* **2020**, *47*, e2020GL087085. [CrossRef]
92. Bintanja, R. The impact of Arctic warming on increased rainfall. *Sci. Rep.* **2018**, *8*, 16001. [CrossRef] [PubMed]
93. Bjorkman, A.D.; Criado, M.G.; Myers-Smith, I.H.; Ravolainen, V.; Jónsdóttir, I.S.; Westergaard, K.B.; Lawler, J.P.; Aronsson, M.; Bennett, B.; Gardfjell, H.; et al. Status and trends in Arctic vegetation: Evidence from experimental warming and long-term monitoring. *Ambio* **2020**, *49*, 678–692. [CrossRef] [PubMed]